We are IntechOpen, the world's leading publisher of Open Access books Built by scientists, for scientists

4,800
Open access books available

122,000
International authors and editors

135M
Downloads

Our authors are among the

154
Countries delivered to

TOP 1%
most cited scientists

12.2%
Contributors from top 500 universities

CLARIVATE ANALYTICS BOOK CITATION INDEX INDEXED

WEB OF SCIENCE™

Selection of our books indexed in the Book Citation Index in Web of Science™ Core Collection (BKCI)

Interested in publishing with us?
Contact book.department@intechopen.com

Numbers displayed above are based on latest data collected.
For more information visit www.intechopen.com

13

Net-Shaping of Ceramic Components by Using Rapid Prototyping Technologies

Xiaoyong Tian[1], Dichen Li[1] and Jürgen G. Heinrich[2]
[1]*Xi'an Jiaotong University, Xi'an,*
[2]*Clausthal University of Technology, Clausthal-Zellerfeld,*
[1]*China*
[2]*Germany*

1. Introduction

The application of rapid prototyping (RP) in ceramics was motivated by the advances in engineering ceramics and traditional ceramics where methods of creating complex shapes are limited (Cawley, 1997). Ceramics have many outstanding physical and chemical properties and attract lots of researchers' attentions to find new industrial applications for this kind of material such as components resistant to the high temperature, piezoelectric sensor and actuators (Safari et al., 2006; Miyamoto, 2004). But ceramics often cause high machining costs for products in limited quantities and high tooling costs in injection molding of large batches. Moreover, ceramic components with complicated structures cannot be shaped by the conventional forming processes such as casting, forging and machining. High temperature ceramics are also hard and difficult to machine. Even for the simple geometries which can be produced by the traditional fabrication process, the time needed for the mould preparation drastically enlarges the period between the design and the first prototyping verification of the new production. Industrial applications of ceramic materials especially for the jobbing work and complicated components are largely restricted by the lack of the net-shaping capability for the components with complex structures.

Rapid prototyping came into being at the end of last century when the first Stereolithography Apparatus (SLA) was invented as the first RP machine in 1984 by 3D Systems (Hul, 1984). It begins with a CAD model, usually a solid or a surface model which can be designed by the users. The CAD model is imported into the rapid prototyping system in which there is special software slicing the solid model to define a group of layers. The layer information including the process route, parameters and material properties is read by the computer. A computer controlled laser scanner realizes the laser scanning process to form each layer according to the respective layer information. Since the object grows layer by layer, it is possible to realize material and process combinations which are impossible to achieve with conventional methods. The general purpose is just to make prototypes in order to reduce the time of products development by shortening the period between design and test and then cut the development cost of new products.

In recent years a pronounced method diversification has resulted in a large variety of different rapid prototyping techniques allowing for the generation of prototypes made of polymers, metals and ceramics. Now functional components, specially using metal or

ceramic materials, are manufactured using rapid prototyping process by lots of researchers and companies all over the world. There are several processes to realize the net or near-net shaping of the ceramic functional components such as stereolithography of the ceramic slurry, extrusion of ceramic paste, fused deposition of using ceramic loaded polymer filament, selective laser sintering of ceramic powder and 3D printing et al. In this chapter, these typical ceramic net-shaping processes are briefly reviewed. Then, direct laser sintering of ceramics by using Layer-wise Slurry Deposition (LSD) process and Lost Mould combined with Reaction Formed Silicon Carbide process will be described in details. At last, all the processes will be compared according to the raw material, efficiency, fabrication accuracy and et al.

2. Net-shaping of ceramics by RP technologies- a review

2.1 Stereolithography (SL) of ceramic slurry

Photocuring is the basis of SL, one of the most popular and most accurate SFF techniques. Commercial SL machines (3D system, CA) produce plastic prototypes from epoxy resins by photo-polymerization of a liquid monomer with a UV laser. For the 3D-fabrication of ceramics via stereolithography the liquid monomer is replaced by "ceramic resin", a suspension of ceramic powder dispersed in a UV-curable resin, first demonstrated by Gritffith and Halloran (Griffith & Halloran, 1996). As shown in Fig. 1, the first step is curing a thin layer (150~200μm) by laser scanning the cross section on the surface of the ceramic resin. The part is attached by supports to an elevator platform beneath the surface of the ceramic resin. After curing the layer, the elevator platform dips into the suspension allowing the liquid ceramic resin to flow over the cured portion of the part. A doctor blade sweeps over the surface leaving a layer of fresh ceramic suspension which becomes the next cured layer after the laser curing process. Repeating this process building up the three dimensional green body of the ceramic components. And then after post sintering in furnace, dense ceramic objects are obtains. Lasers used in current practice are helium cadmium gas lasers, argon ion gas laser and more recently solid state Nd-YVO4 lasers.

T. Chartier et al have investigated the ceramic suspension suitable for the SL process (Chartier et al., 2002; Hinczewski et al., 1998). To achieve a sufficiently high green density in the part, the solid volume fraction should be in the range of 0.50-0.65. On the other hand, a low viscosity is necessary for a proper flow during recoating of the next layer. Alumina and silica powders have been used to prepare the ceramic suspension (Griffith & Halloran, 1996; Chartier et al., 2002; Hinczewski et al., 1998; Tay et al., 2003). Final mechanical strength similar with that of the uniaxial pressed samples has been achieved.

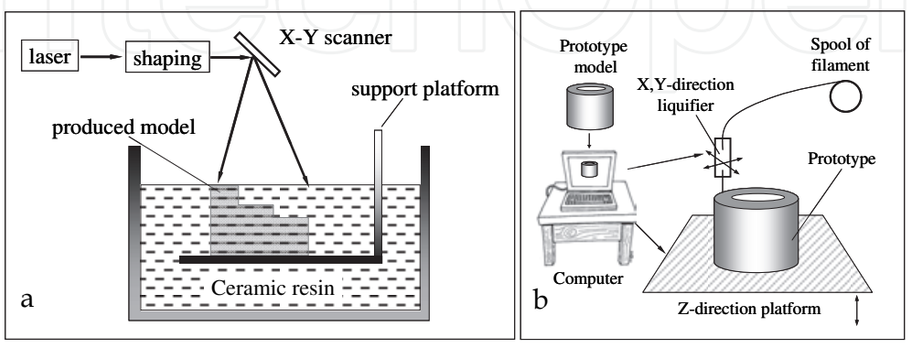

Fig. 1. a) Stereolithography of ceramic powder loaded liquid resin (Griffith & Halloran, 1996), b) Schematic for the extrusion fabrication process (Bandyopadhyay et al., 1997)

2.2 Extrusion forming techniques

The Fused Deposition Manufacturing of Ceramics (FDMC) was developed firstly by Ahmad Safari (Bandyopadhyay et al., 1997; Lous et al., 2000). Filaments were fabricated with a ceramic powder loaded of 50-55vol% in a six-component thermoplastic binder system that contained polymer, elastomer, pacifiers, wax, surfactant, and plasticizer. The filament with a diameter of about 1.8 mm passes through a heated liquefier (140-200^{o}C) and acts thereby as a piston to extrude a continuous bead, or "road' of molten material through a nozzle with a diameter of 0.254-1.5mm (Fig.1 b). The bead is deposited on a platform that indexes down after the first layer is completed. Bonding of neighboring beads and previous deposited layers takes place due to adhesiveness of partly molten material. The 3D components were fabricated by repeat this deposition process layer by layer. After the green part was fabricated, the part was removed from the substrate for further heat treatment processing to remove the organic additives.

Another extrusion forming process of ceramic components, extrusion free forming, developed at the Advanced Research Center (Tucson, AZ, USA) (Lombardi & Calvert, 1999; Vaidyanathan et al., 2000), was equipped with a high pressure extrusion head. This technology has been used for different ceramic materials dispersed in wax-based binders. The fabrication of silicon nitride parts by extrusion of suspensions with as ceramic loading of 55vol% was reported by Baidyanathan et al. [12]. Thermoplastic suspensions of 55vol% zirconia in a wax-based vehicle were extruded through a range of fine nozzles with diameters from 76 to 510μm (Gridal & Evans, 2003). Heat transfer considerations show that the use of thermoplastic suspensions was not ideal for fine (<100μm in diameter.) filament work because the fibers solidified before folding and welding. That means that the use of solid-liquid change materials in extrusion techniques is limited for microfabrication, because the filament solidifies too quickly in ambient air. Solvent-based extrusion freeforming was also developed to build complex ceramic 3D structures. The principle for this technique was transition of the paste from liquid to solid by solvent evaporation (Lu et al., 2010). The drawbacks of solid-liquid change material were overcome.

2.3 Three-dimensional printing

There are two kinds of 3D printing fabricating processes. One is the three-dimensional printing which uses layered ceramic powder and organic binder. Another is the direct ceramic ink-jet printing which uses ceramic powder loaded ink.

Powder based three-dimensional printing was developed at Massachusetts Institute of Technology, USA in 1992 as a method to create preforms from powdered metals and ceramics (Sachs et al., 1992). An individual two-dimensional layer is created by adding a layer of powder to the top of a piston and cylinder which contain a powder bed and the part being fabricated. A new layer of the being built component is to be formed by "ink-jet" printing of a binder material. And then, the piston, powder bed and part are lowered and new layer of powder is spread out and selectively joined. This layering process is repeated until the part is completely printed. After removing the unbound powder, a heat treatment process is following to densify the fabricated part. The sequence of operations is illustrated in Fig.2 a.

Direct ceramic ink-jet printing (DCIJP) makes use of ink-jet printers to create components by multilayer printing of a colloidal suspension dispersed with ceramic powder. This process has the potential to produce a wide range of fine ceramic contours with high resolution enabling miniature components to be manufactured. Functional gradients and multi materials components can be fabricated by this printing method according to the multi

nozzles. By adjusting the aperture of the printing head and by controlling the spreading phenomenon of the droplet, one can expect to reach a standard definition of around 50µm and ultimately of 10µm, taking into account the tremendous evolution in the printing field (Cappi et al., 2008; Lejeune et al., 2009).

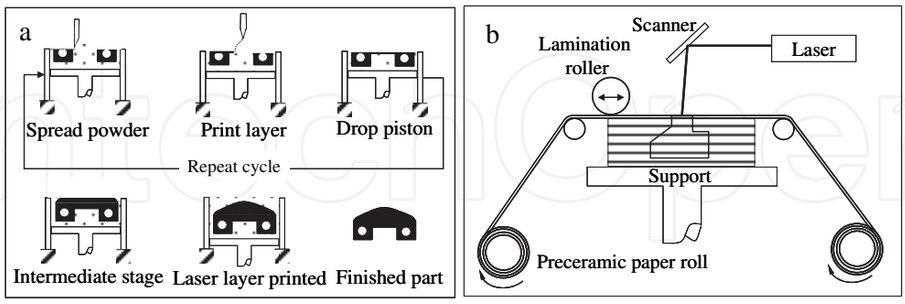

Fig. 2. a) Sequence of operations in the three-dimensional printing process (Sachs et al., 1992), b) Schematic setup of laminated object manufacturing (Travitzky et al., 2008)

2.4 Laminated objective manufacturing

Laminated object manufacturing (LOM) generates three-dimensional ceramic components by sequential stacking, laminating, and shaping of preceramic paper or ceramic green tape (Fig.2 b). It can be considered as a hybrid between additive and subtractive processes: a part is built up in a layer-by-layer lamination approach. Each layer is individually cut by a knife or laser beam according to the cross section of the part defined by the CAD model. Each layer is bonded to the previous layer with a thermoplastic adhesive coating on the bottom side of the paper sheet, which is activated by heat and pressure during the LOM processing. Al_2O_3 and SiC preceramic papers have been prepared for the LOM process (Travitzky et al., 2008). Commercial Low Temperature Co-fired Ceramic (LTCC) green tapes were also used to fabricate complicated ceramic components by Cold Low pressure Lamination [CLPL] process (Schindler & Roosen, 2009). Research on the use of a non-planar LOM process has also been carried out to build curved layer parts to overcome the restriction of flat layers (Klosterman et al., 1999).

2.5 Selective laser sintering

A thin layer powder is spread by a roller from the powder container to the platform, as shown in Fig.3 a. The new powder layer is then selectively sintered by a laser via a scanner controlled by a computer according to the pattern of the cross section in the CAD model. Non-sintered powder is left to serve as a support for the following layers. The laser sintered part is obtained by removing the unsintered powder. For ceramic powders, post treatment is always required to densify the microstructure and achieve a high mechanical property. Oxide ceramic powders, such as alumina and silica, have been selectively sintered by ND: YAG-laser (1064 nm) (Regenfuss et al., 2008). Pure yttria-zirconia powder was also sintered by a fiber laser with a wavelength of 1.064um. But the density and the mechanical properties of the produced samples can not meet the requirement for their potential medical application as dental bridges (Bertrand, 2007). Lower melting point constitutions, such as metal and organic powder were added into the ceramic powder to lower the sintering temperature and then form composite components.

Silicon carbide cannot be reversibly transferred to a liquid state under normal pressure conditions. It decomposes at around 2800-3000^{o}C. The mixed powder of 51% SiC, 41% Si

and 8% C were used for laser micro sintering. The appearance of silicon decreases the sintering temperature because silicon has a melting point around 1420°C. During laser sintering process, melt silicon reacts with carbon and the reaction-formed silicon carbide and residual silicon bind initial silicon carbide powder together (Regenfuss et al., 2008).
Polymer derived ceramic parts with complex shapes were fabricated by selective laser curing (SLC). The ceramic parts were produced by sequentially sintering of SiC loaded polysiloxane powder with a CO_2-laser beam (λ = 10.6um), which locally induces curing reaction of the polymer phase at moderate temperatures around 400°C. The laser-cured bodies were converted to Si-O-C/SiC ceramic parts in a subsequent pyrolysis treatment at 1200°C in argon atmosphere. A post-infiltration with liquid silicon was carried out in order to produce dense parts. The bending strength was only 17MPa before infiltration as a result of both micro cracks in the Si-O-C matrix and a pronounced porosity, while an average value of 220MPa was achieved after post-infiltrating with Si (Friedel et al., 2005).

2.6 Indirect rapid fabrication process

Polymer and wax moulds were produced by using rapid prototyping process, such as SL (Wu et al., 2009; Yin et al., 2004), FDC (Stampfl & Prinz, 2002), and SLS (Guo et al., 2004; Cai et al., 2003) et al., and used for the gel-casting of ceramic slurry to fabricate ceramic components with complex structures. The basic process for the lost mould application of rapid prototyping is shown in Fig.3 b. First, the negative model of the ceramic part was designed in CAD software. Then the negative model was fabricated into a wax or polymer mould by using rapid prototyping process. This polymer mould was used for the gel casting of ceramic slurry which contains monomer, cross linker, imitator, and ceramic powder. After drying, the ceramic slurry was polymerized to form a macromolecular network which binds the ceramic powder together. Enough mechanical strength of the green ceramic body can be achieved for the following treatments. Optimized thermal cycle was applied to the polymerized ceramic green bodies to get the final dense ceramic parts.

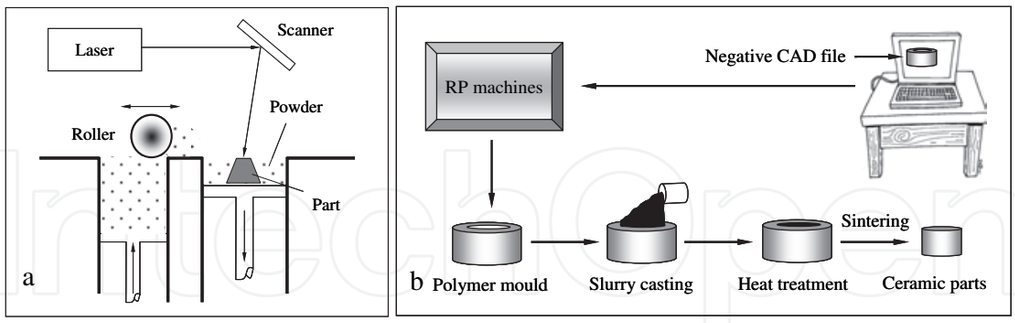

Fig. 3. a) Schematic process of Selective laser sintering, b) Schematic diagram of the steps in the lost mould approach for fabricating ceramic parts

3. Direct laser sintering and layer-wise slurry deposition (LSD)

3.1 Fabrication process

Direct laser sintering using LSD belongs to the selective laser sintering processes except that the starting material in LSD process is ceramic slurry instead of ceramic or polymer-ceramic mixed powders. Layer-wise slurry deposition has been utilized to produce a dense ceramic tape for the following laser sintering process by J. G. Heinrich and colleagues (Sadeghian et

al., 2004; Guenster et al., 2003; Gahler et al., 2006; Heinrich et al., 2007; Krause et al., 2004; Tian et al., 2009). Slurry used in this process is aqueous ceramic suspension with organic additive less than 2% (by the TG analysis). Ceramic tapes can be achieved by evaporating the water in the deposited ceramic slurry layers. These ceramic tapes have a dense microstructure and higher green density than the powder matrix which is used in the conventional selective laser sintering processes. Higher green density will improve the sinteractivity of the ceramic powder and produce a dense laser sintered ceramic body.
The principle of layer-wise slurry deposition (LSD) based direct laser sintering process are illustrated in the Fig. 4. Ceramic slurry is pumped through a doctor blade and deposited on a pre-heated ceramic tile. After drying, the ceramic tape is sintered by a laser beam, which is controlled by a computer via a scanner according to the pattern of the cross sections in the CAD model. Repeat this process until all the layers are finished. The unsintered area is removed by putting the whole part into the water since aqueous ceramic slurries were used. Finally, the laser sintered body is obtained.

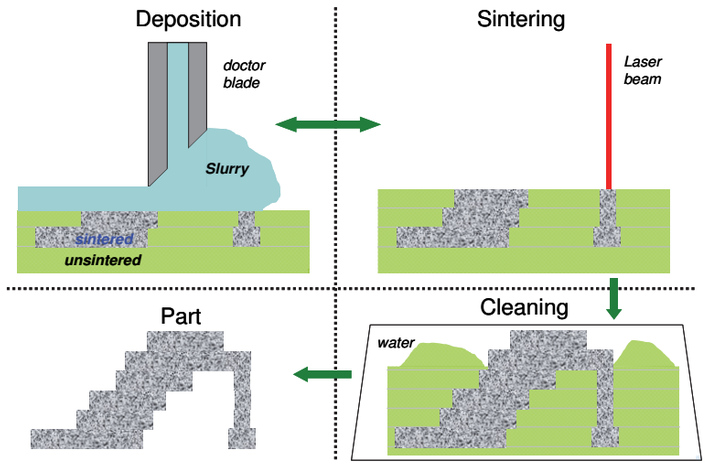

Fig. 4. Fabrication process of ceramic components by using Layer-wise Slurry Deposition and direct laser sintering (Gahler et al., 2006)

3.2 Temperature in heat affected zone (HAZ)

Temperature in HAZ has a significant influence on the microstructure, density and mechanical strength of the laser sintered ceramic bodies. Whereas the temperature in HAZ is affected by the laser sintering process parameters, the relationships between the laser sintering parameters and the sintering temperature become crucial in order to improve or optimize the properties of the laser sintered bodies.
In LSD based laser sintering process, four parameters should be investigated, laser power, scan speed, hatch spacing and layer thickness. However the thickness of newly deposited layer is a constant value of 0.1mm for all experiments in the present research. There are only three factors left to be studied. Laser energy density (LaserED) applied on the surface of the dried slurry is defined as

$$LaserED = \frac{P}{D \times V}(J / cm^2) \tag{1}$$

where P is the laser power, D is the diameter of the laser beam (0.6 mm in diameter) and V is the laser scan speed. The values of P and V are adjustable in the laser sintering process.

A pyrometer was installed in the laser sintering equipments to simultaneously detect the temperature in the heat affected zone (HAZ). The specimens with different sintering temperature were investigated according to the delamination of two adjacent layers or cracks on the surface. An isothermal map of sintering temperature on hatch spacing and laser energy density is plotted in Fig.5. It shows that large laser energy density and small hatch spacing will produce high sintering temperature in the HAZ.

In the inadequate sintering region of Fig. 5 (T<1050°C), the green bodies delaminated due to the low temperature and the consequent low penetration depth. In the inordinate sintering region of Fig. 5 the cracks (Fig. 6b) appeared on the surface of the sintered bodies due to the high temperature (T>1400°C). On the contrary, in the appropriate laser sintering temperature range (around 1050 °C~1400°C in Fig. 5), the laser sintered surface are homogenous and there are no cracks being observed (Fig. 6 a).

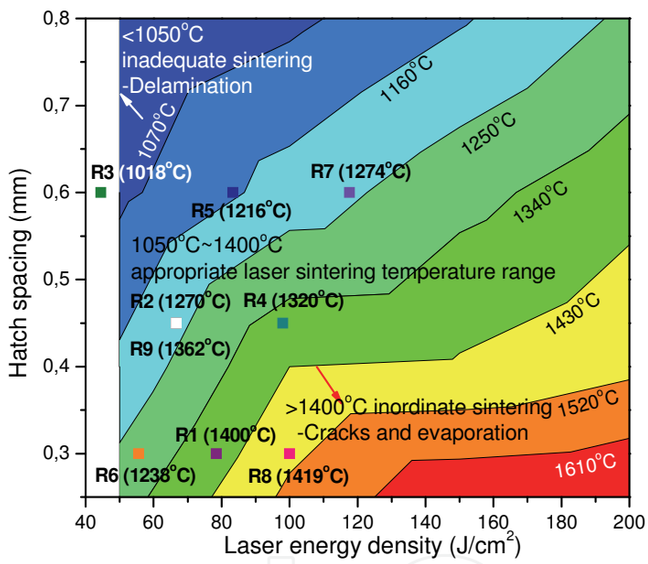

Fig. 5. Influence of laser energy density and hatching space on the temperature in the laser sintering zone, and simulated temperature (average value) for each experimental group

Simulation of the temperature in the HAZ has also been conducted by using the model which has been put forward in the literature (Tian et al., 2010). To validate the feasibility and accuracy of this numerical model, the average laser sintering temperature for each experimental group has been simulated and compared with the experimental results, as shown in Fig. 5. The positions of each experimental group are marked in this isothermal map with the simulated temperature in the following round brackets. The difference between simulated temperature and experimental results is less than around 5%. It can be concluded that simulated temperatures basically match the experimental results. Moreover, the objective of the simulation is a qualitative investigation instead of a quantitive one. It means that this model is reasonable to simulate the laser sintering process of porcelain samples and can be used for the further investigation.

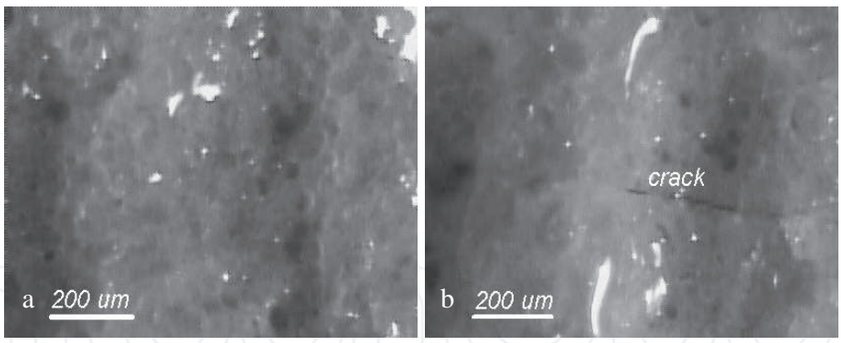

Fig. 6. Optical micrographs of laser sintered surface treated with different laser energy density: a. 125 J/cm²; b. 250 J/cm²

The influence of laser sintering parameters on the average sintering temperature is shown in Fig. 7. With large hatch spacing and low laser energy density (low laser power, and high scan speed) the temperature in the sintering zone decreases. This simulation results are entirely consistent with the experimental results which are shown in Fig. 5.

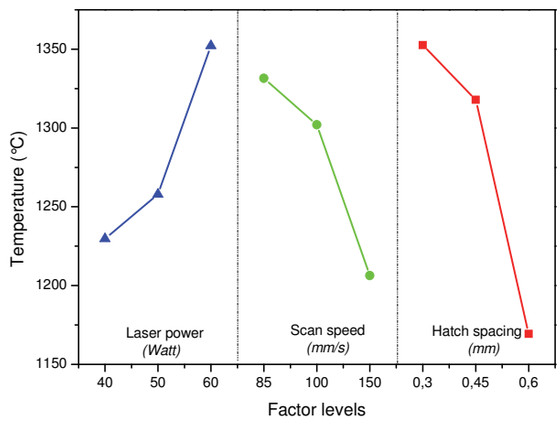

Fig. 7. Average effect of laser sintering parameters on the temperature (statistical results from simulation)

3.3 Residual stresses in the laser sintered bodies

After the laser sintering process is finished, the model is cooled down to room temperature. Transient thermal stresses will be partially released during the cooling process. But there are still residual internal stresses remaining in the model which plays an important role considering the final mechanical strength of ceramic parts after being post sintered in the furnace.

According to the simulation results, distribution patterns of residual internal stresses in x, y, and z directions are shown in Fig. 8 (left). Residual tensile stress appears in the upper part of the model and residual compressive stress appears in the bottom part of the model. This stresses distribution pattern will significantly influence the final mechanical strength of ceramic components. In the real experimental procedure, laser sintered ceramic samples will be post-sintered in a furnace after laser sintering process. In the post sintering process, the stresses with two opposite directions will be released and cause creeps and consequent delamination between two adjacent layers. In the present research, the thickness of the

model is 2mm which is much thicker than one single layer (0.1mm) in the real experiments. Analogy can be made between the simulation model and real experimental situation after 200 layers (2mm in depth) have been deposited on the ceramic tile.

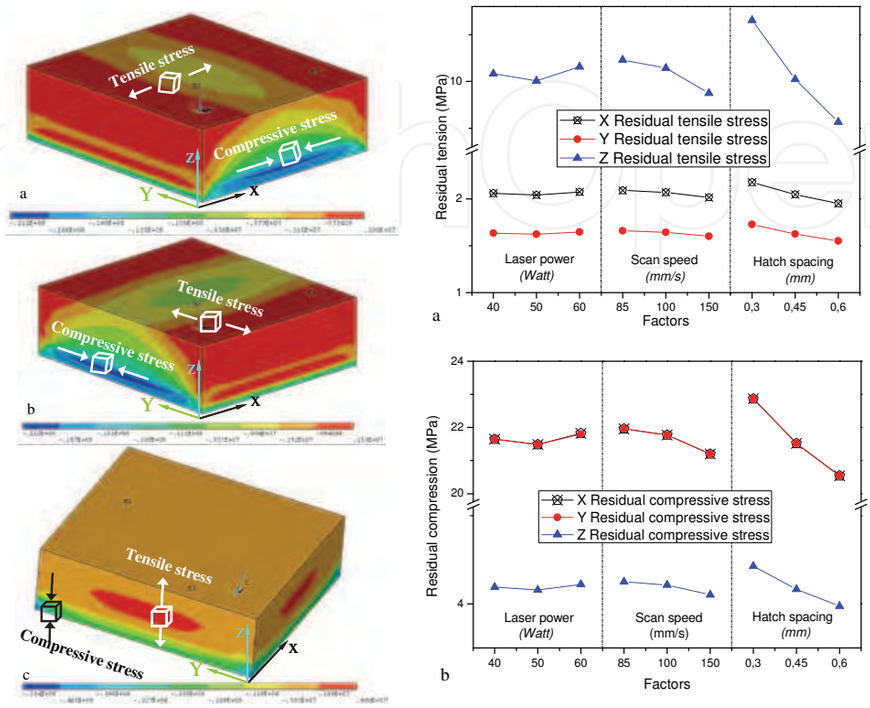

Fig. 8. **Left**, Residual internal stress profiles (Pa) with fully constrained bottom surface, R3, a) X component, b) Y component, c) Z component; **Right**, Average effect of laser sintering parameters on the maximum residual stress, a) tension; b) compression (statistical results from simulation)

Average effects of laser sintering parameters on the maximum residual stresses are shown in Fig. 8 (left). Residual tensile stresses (Fig. 8 (right) a) in z direction (around 10MPa) are much higher than those in x (around 2MPa) and y (around 1MPa) directions. With high laser power and low scan speed, the residual tensile stresses are slightly increased. Hatch spacing has a significant influence on the residual stresses. With large hatch spacing, low residual tensile stresses are present especially for the Z component, as shown in Fig. 8 (right) a. The influence of laser sintering parameters on the residual compressive stresses is similar to that of the residual tensile stresses. X and Y components (around 22MPa) are much higher than the Z component (around 4MPa). Moreover, X component is almost equal to Y component, as shown in Fig. 8 (right) b. In practice, the relationships between laser sintering parameters and residual stresses are more critical than the exact quantity of the stresses. These relationships are very helpful to build up a connection between residual stresses and final mechanical strength of the post sintered ceramic samples.

3.4 Microstructure

In order to understand how the different changing trends of the shrinkages appeared, it is useful to investigate the development of microstructures before (Fig. 10) and after post sintering process (Fig. 9).

The morphology of post sintered specimens was carefully investigated on the fracture cross sections by SEM (Fig. 9). Obvious delaminations are found in R1 and R8 (Fig. 9). The common feature of these two groups is the same hatch spacing of 0.3mm. The laser energy densities of R1 and R8 are 78.43 J/cm^2 and 100 J/cm^2, respectively. These two groups of experiments fall into the inordinate sintering region in Fig. 5 where the sintering temperature is higher than 1400^{o}C. The delamination between two adjacent layers is probably due to the residual thermal stress produced by the laser inordinate sintering. The residual stress couldn't be freely released during the post sintering process. The accumulation of the stresses finally causes the delamination between adjacent layers in the laser sintered body.

On the contrary, the densest microstructure in Fig. 9 is R3 which has a hatch spacing of 0.6 mm and laser energy density of 44.44 J/cm^2 belonging to the inadequate sintering region in Fig. 5. The samples in this group actually delaminated after the laser sintering (Fig. 10a) and it is consistent with the description of Fig. 5. The cross section microstructure in the laser sintered body of R3 is shown in Fig. 10a. There are lots of unsintered regions between two adjacent layers and the binding of the two adjacent layers is relatively loose due to the inadequate laser sintering. When these samples are being post sintered, these remained loose regions could freely release the residual stresses and then tightly combine the adjacent layers together to produce a densified microstructure (Fig. 9 R3). In contrast to the loose binding of the samples in group R3 (Fig.10 a), the microstructure of R5 is more compact (Fig. 10 b). But the post sintered samples in group R3 have a more homogeneous and dense microstructure than the samples in group R5, as shown in Fig. 9. This is consistent with the stress release function of the loose unsintered regions between two adjacent layers.

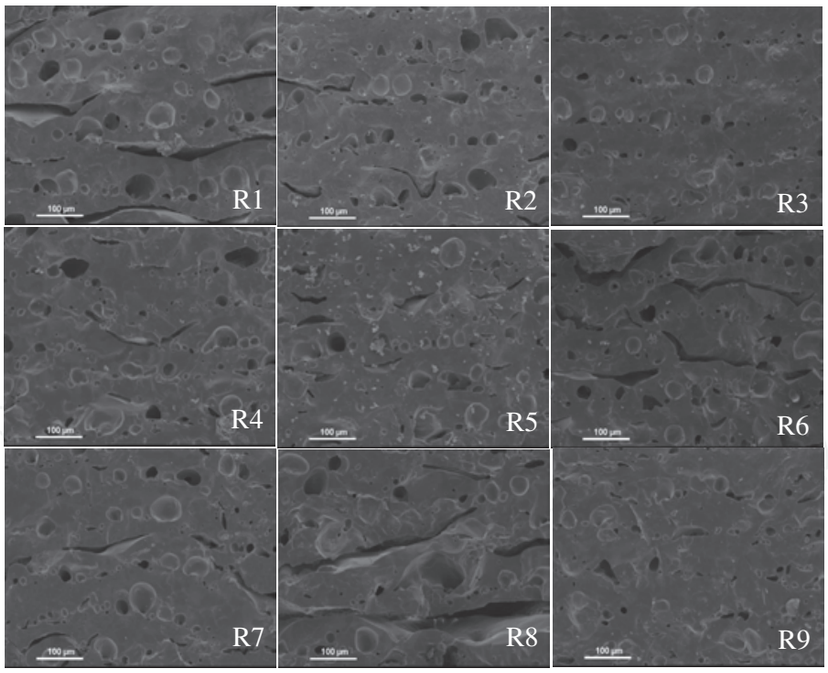

Fig. 9. Microstructure in the fracture cross sections of laser sintered samples after post sintered in a furnace at 1425^{o}C for 2 hours (SEM). The parameters (laser energy density and hatch spacing) used for each group are following:
R1) 78.43J/cm^2, 0.3mm; R2) 66.67J/cm^2, 0.45mm; R3) 44.44J/cm^2, 0.6mm;
R4) 98.04J/cm^2, 0.45 mm; R 5) 83.33J/cm^2, 0.6mm; R6) 55.56J/cm^2, 0.3mm;
R7) 117.65J/cm^2, 0.6mm; R8) 100.0J/cm^2, 0.3mm; R9) 66.67J/cm^2, 0.45mm

A stress relief mechanism was put forward to interpret the changes of the microstructure during the post sintering process and theirs influence on the bending strength (Tian et al., 2010). It has been experimentally proved in the present research that small hatch spacing and high laser energy density will produce high sintering temperature in the HAZ. High transient or residual stress will arise because of the high sintering temperature as well as the large temperature gradient. The post sintering process could be considered as a stress relief process in which residual stress will be released and induce delamination in the ceramic samples. Consequently, the bending strength is reduced by the appearance of delamination which will be discussed in the next section.

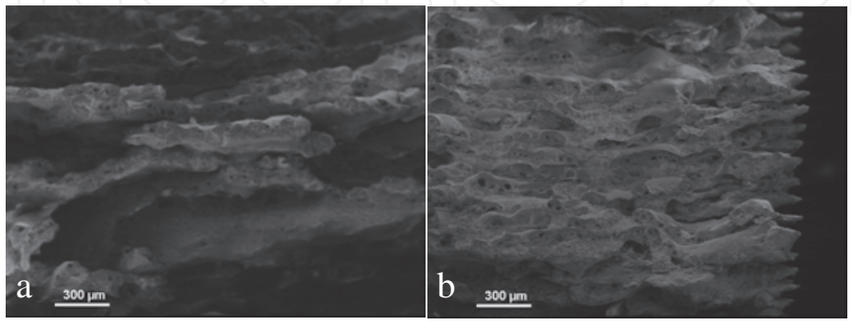

Fig. 10. Microstructures of fracture cross sections in the laser sintered samples (a. R3, b.R5) (SEM)

3.5 Density and mechanical properties

Bulk density and bending strength were measured to study the influence of laser sintering parameters on the properties of final ceramic components. The average effect of laser sintering parameters upon the bending strength is shown in Fig. 11 a. Large hatch spacing and low laser energy density (low laser power and high scan speed) produce high bending strength of the ceramic specimens. The changing pattern of bending strength is consistent with the microstructures shown in Fig. 9. The bulk density is shown in Fig. 11 b. With increasing bulk density the bending strength increases.

The maximum value of bending strength is 29.3±1.0MPa in group R3 which has a most densified microstructure (Fig. 9 R3). However the laser sintered bodies in group R3 delaminated and had a low green strength. The laser sintering parameters in this group cannot be adopted in the following experiments. By comparison with R3, samples in R5 have relatively densified microstructure in the green bodies (Fig. 10b) and relative high bending strength (23.8±1.6MPa, higher than R9 19.5±2.5MPa, as shown in Fig.12) after post sintering. So the laser sintering parameters of group R5, laser power of 50 W, scan speed of 85 mm/s and hatch spacing of 0.6mm, are more appropriate than others.

The relationship between laser energy density and bending strength of the samples post sintered in furnace at 1425^{o}C is shown in Fig. 12. The relation between laser energy density and bending strength is not obvious because bending strength is greatly influenced by hatch spacing. However the maximum bending strength was still achieved when the laser energy density got a minimum value (44.44 J/cm^2, R3). The bending strength was directly measured using the post sintered samples without surface polishing. So the value of the bending strength could be higher after surface treatment.

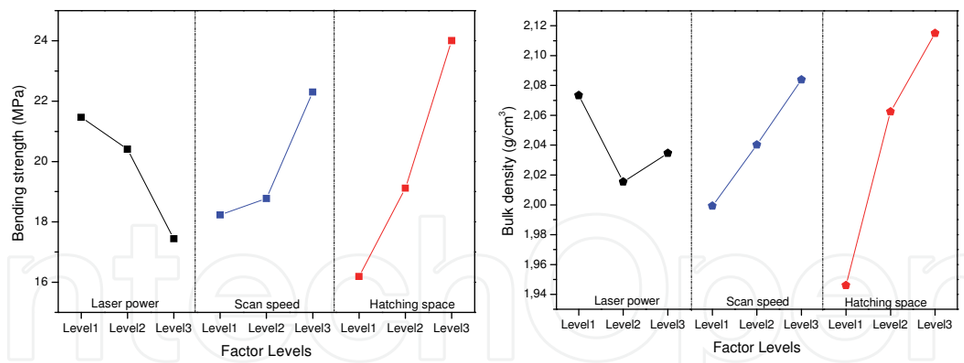

a) b)

Fig. 11. a) Average effect of each laser sintering factor upon the bending strength of the ceramic samples, b) Average effect of each laser sintering factor upon the bulk density of the ceramic samples

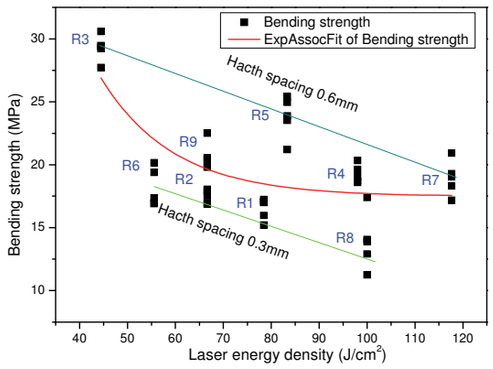

Fig. 12. Relation between laser energy density and the bending strength of the ceramic samples post-sintered in furnace at 1425°C

3.6 Accuracy

The manufacturing accuracy of the direct laser sintered ceramic samples consists of dimensional accuracy in three directions and the surface accuracy. The dimensional accuracy in the laser sintered surface (X, Y plane) depends on the scanning accuracy of the scanner which is controlled by the computer software and can be adjusted or controlled. In Z direction, the dimensional accuracy is affected by the thickness of the deposited slurry layer and the solid content in the slurry, which will be discussed in Section 3.6.1. The surface roughness of the laser sintered plane is controlled by the laser sintering parameters. It's no just an accuracy issue due to the interrelationship between laser sintering parameters and mechanical properties. So, only the influence of surface angle on its roughness will be presented in Section 3.6.2.

3.6.1 Layer thickness

In the fabrication process, a 3D software is used to slice the three-dimensional CAD model from STL files into a series of two-dimensional cross sections. When the layer thickness is

assigned during the slicing process, the cross sections are derived at the increments of that layer thickness. The actual layer for the part is deposited by the stepping of the working table in the same increments. This converts the two-dimensional cross sections into the three-dimensional layers of the actual prototype. The real layer thickness which can be produced by the layer-wise slurry deposition depends on the particle size and the solid content.

The slurry thin film deposited on the preheated ceramic tile will shrink due to the loss of water. Thus the real thickness of each dried layer is different when the preset layer thickness is fixed. The real thickness can be calculated by the following formula,

$$T_l(n) = H(1 - a^n) \tag{2}$$

where $T_l(n)$ is the thickness of the n-th layer after drying, H is the preset slurry deposition thickness (0.1mm in the present research) and a is the shrinking ratio of slurry layer during drying process.

The shrinking ratio (a) of the deposited thin slurry film depends on the volume content of water in the used slurry. The slurries used in the LSD process normally have water content in volume less than 50%. Thus the possible shrinkage ratios for the slurry are less than 50%. The influence of shrinkage ratio on the thickness of dried layers is illustrated in Fig. 13 derived from the Equation x.2. The real thickness is changing at the first few layers and approaching the preset ideal layer thickness, 0.1mm in the present research. More layers are needed to approach the preset thickness for the slurry with large shrinkage ratio. For example, the slurry with a shrinkage ratio of 50% takes 10 layers to achieve 99.9% preset thickness and for shrinkage ratio of 0.1 just 3 layers are needed.

In the fabrication process, supporting layers are always necessary before the laser sintering process starts. The number of supporting layers can also be determined by the shrinkage ratio, i.e. the water content of the slurry. Enough supporting layers can produce homogeneous layer thickness and better quality of the final products.

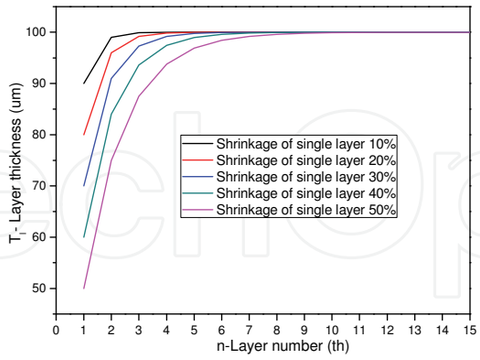

Fig. 13. The development of real layer thickness due to the shrinkage of deposited ceramic slurry

3.6.2 Surface roughness

Surface roughness is quantified by the vertical deviations of a real surface from its ideal form. Roughness is often a good predictor of the performance of a mechanical component, since irregularities in the surface may form nucleation sites for cracks or corrosion.

Ladder effect has a critical influence on the surface roughness of components produced by rapid prototyping. Roughness of curved surfaces is particularly affected by the ladder effect which is the inherent character of layer-wise manufacturing process and can not be avoided. There are two key factors influencing the degree of ladder effect, i.e. surface roughness, layer thickness, and the angle between the slice axis (fabrication direction) and tangent plane of a curved surface, named as surface angle.

In the present research, layer thickness is fixed to 0.1mm. Thus, the dependence of surface roughness on the surface angle will be studied in this section. Ten models with surface angles from 0o to 90^o have been designed, as shown in Fig. 14 a. All the models were input into the rapid prototyping machine (LSD100, Yb-fiber laser system) to fabricate the laser sintered components. Surface roughness measurements were conducted on these samples by using a profilometer along the measuring direction shown in Fig. 14 a. The scan length is 5000μm. Two of them are special, the 0^o surface and 90^o surface. The former is the laser sintered surface and latter is vertical side surface of the component.

Linear profiles of surfaces with different surface angles are shown in Fig. 14 b. Ladder effect is obvious especially for the surface with a small angle (10^o). The vertical side surface with 90^o angle has the smoothest surface because ladder effect has no influence on this surface. The laser sintered surface with 0^o angle has a relative smooth surface because the textured surface was produced by the laser sintering and there was no ladder effect on this surface.

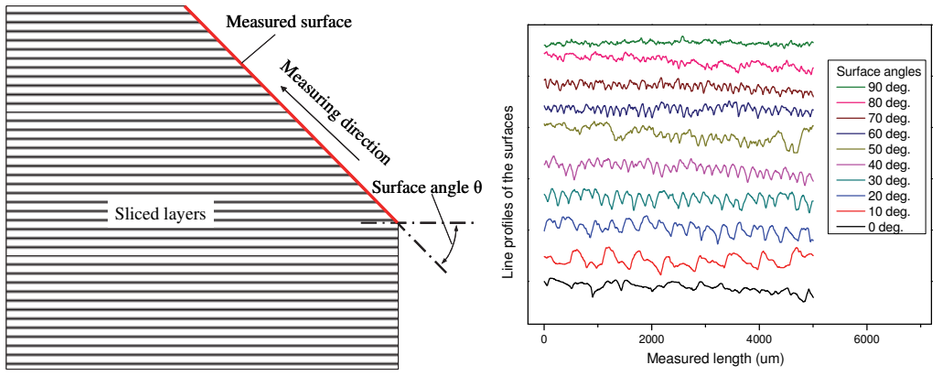

a) b)

Fig. 14. a) Schematic of the surface angle θ from 0 to 90^o , b) Surface profiles with different surface angles

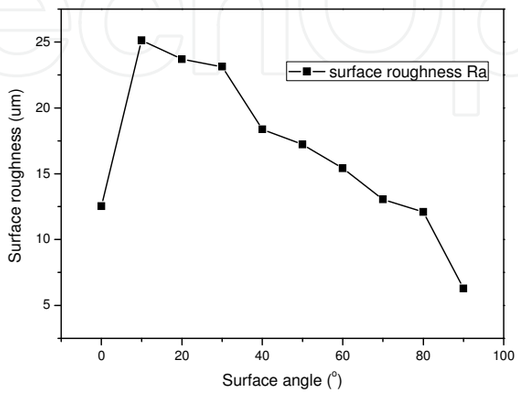

Fig. 15. Surface roughness vs. surface angle

The influence of surface angle on the Ra is shown in Fig. 15. Ra is decreasing from 25.12µm to 12.09µm with an increasing surface angle from 10° to 80° due to the ladder effect. The laser sintered surface hold a Ra of 12.71µm and the vertical side surface has the minimal value of Ra 6.28µm. According to these results from the profilometer, the Ra is variable in the different regions on a curved surface and causes an inhomogeneous surface quality. Post treatment such as surface polishing, and glazing could be used to improve the surface accuracy if necessary.

3.7 Potential applications

3.7.1 Prototypes of porcelain products

Prototypes of the porcelain products are required for evaluation before introducing a new or customized design into the market. The ability to deliver such prototypes in a reasonable time and at an acceptable price can be a decisive factor in a competitive market. However conventional ceramic fabrication processes have the disadvantage that they are normally suitable for the mass production instead of fast and economical manufacturing of prototypes or small-scale series. Porcelain slurry especially for the conventional slip casting process can be taken from ceramic factories and directly used in the present LSD process to produce prototypes of a new design. The cost and lead time for the prototypes can be reduced drastically due to the needless of moulds which are always used in the conventional processes. A bowl model has been fabricated on the LSD 100 machine, as shown in Fig. 16 (left). Certainly, customized ceramic artworks with a complex design like the double-heart in Fig. 16 (right) were also produced by using this LSD process. It probably provides a new method for the artists to transfer their ideas into real ceramic artworks in a very short time.

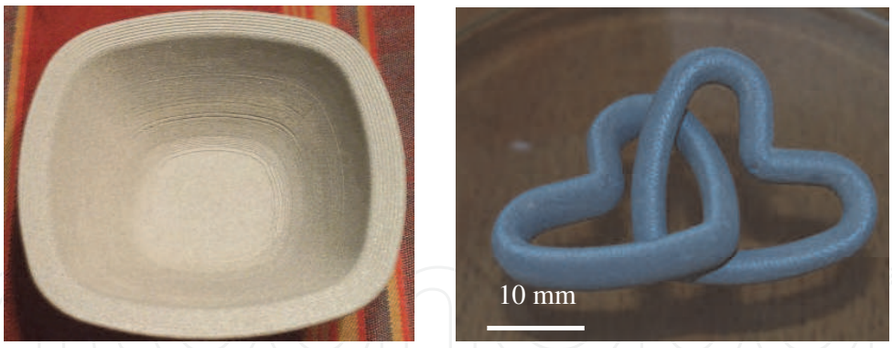

Fig. 16. Porcelain products produced by the LSD-based direct laser sintering process, a bowl (left) and double-heart (right)

3.7.2 Miniature ceramic devices

Several attributes of ceramics make them recognized members in the circles of materials for current and future micro systems. In severe environments, such as high temperature, high pressure, and chemical corrosion, ceramics show very good physical and chemical properties. Moreover, the unique magnetic, piezoelectric, and electro-optical properties make ceramics very popular in the fabrication field of sensors and actuators.

Miniature ceramic parts with a feature size of 500µm have been fabricated by using the LSD-based direct laser sintering process, as shown in Fig. 17. In the following work, high

dielectric constant material can be used by this process to fabricate photonic crystal devices for the microwave application of directional antenna. Piezoelectric ceramics will be used to produce sensors and actuators integrated into a micro system. Laser sinterability of KNN material has already been studied in this thesis. Related research work will continue in the future.

Fig. 17. Miniature ceramic parts by LSD-based direct laser sintering process, photonic crystal, blade wheel, and stationary blade

3.7.3 Biotechnology

The ideal bone implant is a material matrix that will form a secure bond with the tissues by allowing, and even encouraging new cells to grow and penetrate. The used materials should be osteophilic and porous so that new tissue and ultimately new bone can grow into the pores and help to prevent loosening and movement of the implant. As a consequence, a great deal of effort has been placed in the development of porous scaffolds for bone replacement and tissue engineering.

A porous scaffold (Fig. 18) has been fabricated by using porcelain slurry to demonstrate the possible application of our ceramic rapid prototyping machine in biotechnology fields. The model could be reconstructed using the image data from the CT machine. Bioceramics such as hydroxyapatite could be used by the LSD-based direct laser sintering process to produce scaffold for the tissue engineering and bone implants in the future.

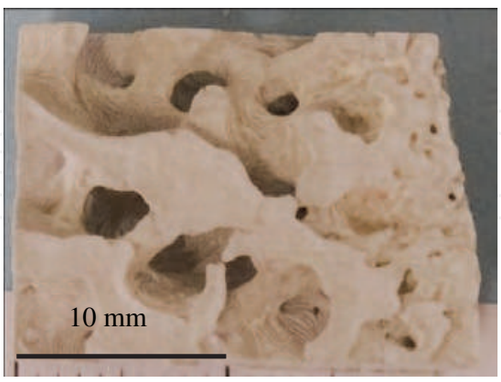

Fig. 18. Porous bone scaffolds

4. Brief comparison of fabrication processes

A simple comparison of these ceramic net-shaping processes will be made according to the following aspects: starting material, energy consumption, efficiency, manufacturing

accuracy, functionality of produced components, and the possibility of materials modification.

4.1 Starting materials

Ceramic slurries are used in stereolithography, direct ink-jet printing, and LSD based laser sintering. For different fabrication process, the content and functions of each composition in the slurry are different. The solid content and viscosity of the ceramic slurry should be optimized according to different process characters. Ceramic powder is used in the three dimensional printing and selective laser sintering process. The powder qualities, such as particle size distribution, morphology, and purity have a great influence on the fabrication processes and properties of produced components. Ceramic tape is used in the LOM process and can be prepared by using the conventional tape casting process. Therefore, it is easy to be adopted by the traditional ceramic factories that have substantial experience on the ceramic tape preparation. Ceramic pastes or filaments are utilized in the extrusion process. The composition and fluidity are important and should be optimized to improve the properties of the ceramic parts. In summary, it is easy to access the ceramic powders as the starting material. Other starting materials, slurry, paste et al, need sequent preparation processes. Aqueous ceramic slurry is widely used in the conventional ceramic manufacturing processes like slip casting and can be directly used by the LSD process. However, the rest slurries, pastes as well as filaments should be prepared carefully by using the ceramic powders.

4.2 Energy consumption

Almost all the rapidly manufactured ceramic parts need post treatment in furnace to further densify the microstructures. So, the difference in energy consumption for each process depends on the characteristics of the material (melting point) and methods used in the shaping processes. Laser employed processes (SL, SLS et al) always consume more energy than the electrical heating process due to the high energy consumption of the laser equipment. Among the laser employed fabrication process, the direct laser sintering of ceramics which always have high densification temperature consumes more energy than the rest processes. In the non-laser processes, the extrusion of ceramic paste consumes less energy than the rests.

4.3 Efficiency

The elemental units in the rapid fabrication process are point, line, face and volume. Different elemental unit causes the diversity of manufacturing efficiency for each fabrication process. “Point” unit is utilized in SL, 3D printing and SLS. “Line” unit is employed in the extrusion process. And LOM process adopts “face” unit as the starting point of the fabrication process. Indirect ceramic forming processes which combine rapid modeling and gel casting use “Volume” as the basic unit. But the efficiency of mould fabrication process should be included into the indirect ceramic forming process. So, LOM process by using “Face” as the basic unit possesses the highest efficiency according to the category of elemental fabrication units. The strategy of the movements in the apparatus also has an influence on the efficiency. Optical movement (laser beam controlled by scanner) has a much higher efficiency than the mechanical movement, such as a knife used to cut the sheets in LOM process.

4.4 Functionality of produced components

Even though there are lots of rapid manufacturing processes focused on the fabrication of ceramic components, functional ceramic parts are still difficult to be produced by most of these processes. Until now, only the indirect rapid manufacturing of ceramic parts by using rapid modeling and gel casting have been used to prepare ceramic parts, such as ceramic shells for the casting. Dense microstructure, high manufacturing accuracy, and good mechanical properties should be achieved before the rapid manufactured ceramic parts can be directly put into the real engineering applications.

4.5 Manufacturing accuracy

Surface accuracy of rapid prototyping depends on the ladder effect which is induced by the principle of fabrication process, slicing and layer-wise deposition. The most important factor influencing the surface accuracy is the layer thickness. Large layer thickness will cause significant ladder effect, especially for the surface with a high curvature. Reducing the layer thickness probably decreases the ladder effect and increase the surface accuracy. But the minimal layer thickness depends on the raw material characters, such as powder size distribution, viscosity of slurry and paste.

Most rapid manufactured ceramic parts need to be post treated in the furnace to densify the microstructure and improve the mechanical strength. Shrinkage in the post treatment process dominates the final dimensional accuracy, which is effected by the different solid content of the starting material in each rapid prototyping process. Dimensional compensation can be used to achieve the ceramic components with the desired size. The information about the shrinkage in the post treatment should be obtained before the accurate compensation can be executed.

4.6 Materials modification

Among all the ceramic solid freeform fabrication processes, only direct laser sintering can manipulate the material properties due to the rapid heating and cooling rate. In the present research, porcelain and $K_{0.5}Na_{0.5}NbO_3$ were both sintered by a laser beam. Dense and textured microstructure has been obtained on KNN samples, which was expected to improve the final piezoelectric properties.

5. Conclusion

In this chapter, net-shaping processes of ceramic components were briefly reviewed. The LSD based direct laser sintering process has been elaborated in details. Temperature distribution in the HAZ was investigated experimentally and by simulation to study its influence on the properties of the produced ceramic components. Microstructure, density and mechanical properties were measured to evaluate and optimize the process parameters. A stress relief mechanism was proposed to explain the relationships between the sintering temperature, residual stresses and microstructure as well as the final mechanical properties. Manufacturing accuracy, including dimensional accuracy and surface roughness, was also studied in order to obtain the desired ceramic components. Some potential applications of the LSD process were also put forward for the future possible researches. A brief comparison has been conducted among all the ceramic net-shaping process at the end of the chapter to help the readers choose appropriate process for their applications.

6. References

Bandyopadhyay, A.; Panda, R. K.; Janas, V. F.; Agarwala, M. K.; Danforth, S. C. & Safari, A. (1997). Processing of piezocomposites by fused deposition technique, *J. Am. Ceram. Soc.*, 80, 1366–72.

Bertrand, Ph.; Bayle, F.; Combe, C.; Goeuriot, P. & Smurov, I. (2007). Ceramic components manufacturing by selective laser sintering, *App. Surf. Sci.*, 254, 898-992.

Cai, K. Guo, D. Huang, Y. & Yang, J. (2003). Solid freeform fabrication of alumina ceramic parts through a lost mould method, *J. Euro. Ceram. Soc.*, 23, 921–925.

Cappi, B.; Oezkol, E.; Ebert, J. & Telle, R. (2008). Direct inkjet printing of Si_3N_4: Characterization of ink, green, bodies and microstructure, *J. Euro. Ceram. Soc.*, 28, 2625–2628.

Cawley, J. D. (1997). *Proc. Int. Gas Turbine and Aeroengine Congress and Exhibition*, Orlando, FA, 1-6, American society of Mechanical Engineering, New York

Chartier, T.; Chaput, C.; Doreau, F. & Loiseau, M. (2002). Stereolithography of structural complex ceramic parts, *J. Mater. Sci.*, 37, 3141-3147.

Friedel, T.; Travitzky, N.; Niebling, F.; Scheffler, M. & Greil, P. (2005). Fabrication of polymer derived ceramic parts by selective laser curing, *J. Euro. Ceram. Soc.*, 25, 193–197.

Gahler, A.; Guenster, J. & Heinrich, J. G. (2006). Direct laser sintering of Al_2O_3-SiO_2 dental ceramic components by layer-wise slurry deposition, *J. Am. Ceram. Soc.* 89, 3076-3080.

Grida1, I. and Evans, J. R.G. (2003). Extrusion free forming of ceramics through fine nozzles, *J. Euro. Ceram. Soc.*, 23, 629–635.

Griffith, M. L. & Halloran, J. W. (1996). Freeform fabrication of ceramics via stereolithgraphy, *J. Am. Ceram. Soc.*, 79, 2601-2608.

Guenster, J.; Engler, S. & Heinrich, J. G. (2003). Forming of complex shaped ceramic products via layer-wise slurry deposition (LSD), *Bul. Eur. Ceram. Soc.*, 1, 1-4.

Guo, D.; Li, L.; Cai, K.; Gui, Z. & Nan, C. (2004). Rapid prototyping of piezoelectric ceramics via selective laser sintering and gel casting, *J. Am. Ceram. Soc.*, 87, 17-22.

Heinrich, J. G.; Gahler, A.; Guenster, J.; Schmuecker, M.; Zhang, J.; Jiang, D. & Ruan, M. (2007). Microstructural evolution during direct laser sintering in the Al_2O_3-SiO· system, *J. Mater. Sci*, 42, 5307-5311.

Hinczewski, C.; Corbel, S. & Chartier, T. (1998). Ceramic suspensions suitable for stereolithogiaphy, *J. Euro. Ceram. Soc.*, 18, 583-590.

Hul, C.H. (1984). Apparatus for production of 3D objects by stereolithography, 3D Systems, US Pat. 4,575,330.

Klosterman, D. A.; Chartoff, R. P.; Osborne, N. R.; Graves, G. A.; Lightman, A.; Han, G.; Bezeredi, A. & Rodrigues, S. (1999). Development of a curved layer LOM process for monolithic ceramics and ceramic matrix composites, *Rapid Prototyping J.*, 5, 61–71.

Krause, T.; Engler, S.; Günster, J. & Heinrich, J. G. (2004). Process and a device for producing ceramic molds. *US Patent Appl.*, 6,827-988

Lejeune, M. & Chartier, T.; Dossou-Yovo, C. & Noguera, R. (2009). Ink-jet printing of ceramic micro-pillar arrays, *J. Euro. Ceram. Soc.*, 29, 905–911.

Lombardi, J.L. and Calvert, P. (1999). Extrusion freeforming of nylon 6 materials, *Polymer*, 40, 1775–1779.

Lous, G. M.; Cornejo, I. A.; McNulty, T. F.; Safari, A. and Danforth, S. C. (2000). Fabrication of piezoelectric ceramic/polymer composite transducers using fused deposition of ceramics, *J. Am. Ceram. Soc.*, 83, 124–28.

Lu, X.; Lee, Y.; Yang, S.; Hao, Y.; Evans, J. R.G. & Parini, C. G. (2010). Solvent-based paste extrusion solid free forming, *J. Euro. Ceram. Soc.*, 30, 1–10.

Miyamoto, Y.; Kirihara, S.; Kanehira, S.; Takeda, M. W.; Honda, K.; & K. Sakoda, (2004). Smart processing development of photonic crystals and fractals. *Int. J. Appl. Ceram. Technol.*, 1, 40-48.

Regenfuss, P.; Streek, A.; Ullmann, F.; Suess, T.; Hartwig, L.; Horn, M.; Kuehn, Ch.; Ebert, R. & Exner, H. (2008). Laser micro sintering of ceramics- reaction models and results, *cfi/Ber. DKG*, 85, 65-72.

Regenfuss, P.; Streek, A.; Ullmann, F.; Kuehn, C.; Hartwig, L.; Horn, M.; Ebert, R. & Exner, H. (2008). Laser micro sintering of ceramic materials, *Part 2, Interceram*, 57, 6-9.

Sachs, E.; Cima, M.; Williams, P.; Brancazio, D. & Cornie, J. (1992). Three dimensional printing: rapid tooling and prototyping directly from a CAD model, *J. Eng. Ind.*, 114, 481-488.

Sadeghian, Z.; Heinrich, J. G. & Moztdarzadeh. F. (2004). Direct laser sintering of hydroxyapatite implants by layer-wise slurry deposition (LSD), *cfi/Ber. DKG*, 82, E1-E5.

Safari, A.; Allahverdi, M. & Akdogan, E. K. (2006). Solid freeform fabrication of piezoelectric sensors and actuators. *J. Mater. Sci.*, 41, 177-198.

Schindler, K. & Roosen, A. (2009). Manufacture of 3D structures by cold low pressure lamination of ceramic green tapes, *J. Euro. Ceram. Soc.*, 29, 899–904.

Stampfl, J. & Prinz, F. B. (2002) Rapid prototyping and manufacturing by gelcasting of metallic and ceramic slurries, *Mater. Sci. and Eng. A*, 334, 187–192.

Tay, B. Y.; Evans, J. R. G. & Edirisinghe, M. J. (2003). Solid freeform fabrication of ceramics, *Int. Mat. Rev.*, 48, 341-370.

Tian, X.; Sun, B.; Heinrich, J. & Li, D. (2010). Stress relief mechanism in layer-wise laser directly sintered porcelain ceramics, *Mater. Sci. Eng. A*, 527, 1695-1703.

Tian, X.; Günster, J.; Melcher, J.; Heinrich, J. & Li, D. (2009). Process parameters analysis of direct laser sintering and post treatment of porcelain components using Taguchi's method, *J. Euro. Ceram. Soc.*, 29, 1903-1915.

Tian, X. (2010). *Rapid* prototyping *of ceramics by direct laser sintering, Papierflieger Verlag GmbH*, ISBN 978-3-86948-107-4, Clausthal-Zellerfeld, Germany.

Travitzky, N.; Windsheimer, H.; Fey, T. & Greil, P. (2008). Preceramic paper-derived Ceramics, *J. Am.* Ceram. *Soc.*, 91, 3477–3492.

Vaidyanathan, R.; Walish, J.; Lombardi, J. L.; Kasichainula, S.; Calvert, P. & Cooper, K. C. (2000). The extrusion free forming of functional ceramic prototypes, *JOM – J. Min. Met. Mat. Soc.*, 52, 34–37.

Wu, H.; Li, D.; Tang, Y.; Sun, B. & Xu, D. (2009). Rapid fabrication of alumina-based ceramic cores for gas turbine blades by stereolithography and gelcasting, *J. Mater. Proc. Tech.*, 209, 5886-5891.

Yin, H.; Kirihara, S. & Miyamoto, Y. (2004). Fabrication of ceramic photonic crystals with diamond structure for microwave applications, *J. Am. Ceram. Soc.*, 87, 598–601.

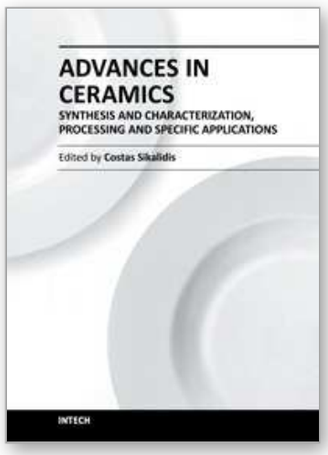

Advances in Ceramics - Synthesis and Characterization, Processing and Specific Applications

Edited by Prof. Costas Sikalidis

ISBN 978-953-307-505-1
Hard cover, 520 pages
Publisher InTech
Published online 09, August, 2011
Published in print edition August, 2011

The current book contains twenty-two chapters and is divided into three sections. Section I consists of nine chapters which discuss synthesis through innovative as well as modified conventional techniques of certain advanced ceramics (e.g. target materials, high strength porous ceramics, optical and thermo-luminescent ceramics, ceramic powders and fibers) and their characterization using a combination of well known and advanced techniques. Section II is also composed of nine chapters, which are dealing with the aqueous processing of nitride ceramics, the shape and size optimization of ceramic components through design methodologies and manufacturing technologies, the sinterability and properties of ZnNb oxide ceramics, the grinding optimization, the redox behaviour of ceria based and related materials, the alloy reinforcement by ceramic particles addition, the sintering study through dihedral surface angle using AFM and the surface modification and properties induced by a laser beam in pressings of ceramic powders. Section III includes four chapters which are dealing with the deposition of ceramic powders for oxide fuel cells preparation, the perovskite type ceramics for solid fuel cells, the ceramics for laser applications and fabrication and the characterization and modeling of protonic ceramics.

INTECH
open science | open minds

InTech Europe
University Campus STeP Ri
Slavka Krautzeka 83/A
51000 Rijeka, Croatia
Phone: +385 (51) 770 447
Fax: +385 (51) 686 166
www.intechopen.com

InTech China
Unit 405, Office Block, Hotel Equatorial Shanghai
No.65, Yan An Road (West), Shanghai, 200040, China
中国上海市延安西路65号上海国际贵都大饭店办公楼405单元
Phone: +86-21-62489820
Fax: +86-21-62489821

IntechOpen